Beach, Dune, and Nearshore Analysis of Southern Texas Gulf Coast Using Chiroptera LIDAR and Imaging System

Authors: Caudle, Tiffany L., Paine, Jeffrey G., Andrews, John R., and Saylam, Kutalmis

Source: Journal of Coastal Research, 35(2) : 251-268

Published By: Coastal Education and Research Foundation

URL: https://doi.org/10.2112/JCOASTRES-D-18-00069.1

Journal of Coastal Research	35	2	251–268	Coconut Creek, Florida	March 2019

Beach, Dune, and Nearshore Analysis of Southern Texas Gulf Coast Using Chiroptera LIDAR and Imaging System

Tiffany L. Caudle*, Jeffrey G. Paine, John R. Andrews, and Kutalmis Saylam

Bureau of Economic Geology, Jackson School of Geosciences
The University of Texas at Austin
Austin, TX 78713, U.S.A.

www.cerf-jcr.org

www.JCRonline.org

ABSTRACT

Caudle, T.L.; Paine, J.G.; Andrews, J.R., and Saylam, K., 2019. Beach, dune, and nearshore analysis of southern Texas Gulf Coast using Chiroptera LIDAR and imaging system. *Journal of Coastal Research,* 35(2), 251–268. Coconut Creek (Florida), ISSN 0749-0208.

LIDAR data and color infrared aerial imagery were acquired for southern Padre Island and Brazos Island, Texas, in 2013 to calculate rates of shoreline change; analyze beach-dune system volume; and test bathymetric LIDAR capabilities along the Texas Gulf of Mexico shoreline. Data were acquired using a Chiroptera airborne system, which simultaneously collects topographic and bathymetric LIDAR and high-resolution imagery. Shoreline position was extracted from LIDAR digital elevation models (DEMs) to compare with historical shoreline positions for shoreline change analyses. Long-term rates (1937–2013) of gulf shoreline change for southern Padre Island and Brazos Island averaged 2.2 m/y of retreat, with 86% of sites retreating. Retreat rates decreased over the last decade (2000–13) to 1.1 m/y (76% of sites retreating). The trend changed between 2010 and 2013: 64% of monitoring sites advanced at an average distance of 4.9 m. Beach and dune volumes above threshold elevations (1 to 6 m above mean sea level) were extracted from DEMs to assess geographic and temporal patterns of sand storage. The undeveloped area of southern Padre Island had 2 to 4 times the volume of sand at lower threshold elevations and 7 times the volume at higher elevation thresholds than did the heavily developed southernmost section of the island. A constant trend across the study area is that volume reduced by approximately half with each 1 m increase in threshold elevation. Beach and dune system volume in the study area increased steadily since 2000, mirroring the decreased retreat rates observed in the shoreline movement analysis. Possible causes of the decreased shoreline retreat rates and increased subaerial sand storage are a lack of tropical cyclone impacts to the study area during the most recent periods, as well as sediment contribution from beach nourishment activities. Bathymetric LIDAR detected the seafloor in low-turbidity areas less than 4 m deep.

ADDITIONAL INDEX WORDS: *Coastal change, sediment volume, beach processes, remote sensing, shoreline change.*

INTRODUCTION

Shoreline position is a critical parameter that reflects the balance among several important processes, including sea-level rise, land subsidence, sediment influx, littoral drift, and storm frequency and intensity. Because the Texas coast, and especially southern Padre Island (Figure 1), faces ever-increasing developmental pressures as the coastal population swells, accurate and frequent analyses of shoreline change will serve as planning tools with which to identify areas of habitat loss; better quantify threats to residential, industrial, and recreational facilities and transportation infrastructure; and help understand the natural and anthropogenic causes of shoreline change.

Trends in shoreline change rates are a critical component in understanding the potential impact that sea level, subsidence, sediment supply, and coastal engineering projects might have on sensitive coastal environments such as beaches, dunes, and wetlands. Rapidly eroding shorelines threaten coastal habitat and recreational, residential, transportation, and industrial infrastructure and can also significantly increase the vulnerability of coastal communities to tropical storms. Repeated, periodic assessments of shoreline position, rate of change, and factors contributing to shoreline change give citizens, organizations, planners, and regulators an indication of expected future change and help to determine whether those changes are accelerating, decelerating, or continuing at the same rate as past changes.

This study discusses short-term, decadal-scale, and long-term shoreline change and beach-dune system volumetric analyses of southern Padre Island and Brazos Island, Texas (southern Texas Gulf Coast), determined from an airborne LIDAR survey conducted by the Bureau of Economic Geology (BEG) in February 2013. The survey mapped a swath about 500 m wide along the shoreline between Mansfield Channel and the Rio Grande (Figure 1). High-resolution color-infrared aerial photography and bathymetric LIDAR data were captured simultaneously. Sand storage and short-term changes were obtained through a volumetric analysis.

Historical change rates of the south Texas Gulf Coast were first determined by the BEG in the 1970s and presented in a series of publications separated at natural boundaries along the approximately 530 km of shoreline (Morton, 1977; Morton and Pieper, 1975). This publication series presented net long-term change rates determined from shoreline positions documented on 1850 to 1882 topographic charts published by the U.S. Coast and Geodetic Survey (Shalowitz, 1964) and aerial photographs acquired between about 1930 and 1975. Rates of change for the entire gulf shoreline were updated through 1982 on the basis of aerial photographs (Morton and

DOI: 10.2112/JCOASTRES-D-18-00069.1 received 1 March 2019; accepted in revision 12 September 2018; corrected proofs received 14 November 2018; published pre-print online 3 January 2019.
*Corresponding author: tiffany.caudle@beg.utexas.edu

Paine, 1990; Paine and Morton, 1989). LIDAR-derived shoreline positions in 2000–01 were used as part of a gulf-wide assessment of shoreline change that included the Texas coast (Morton, Miller, and Moore, 2004, 2005). Coast-wide rates of historical shoreline change were recently updated using 2007 aerial photographs, the most recent coast-wide coverage predating Hurricane Ike in 2008 (Paine, Mathew, and Caudle, 2011, 2012), and 2010, 2011, and 2012 LIDAR data (Paine, Caudle, and Andrews, 2013, 2014, 2017). Through all of these studies, BEG researchers have documented that the Gulf of Mexico shoreline along the southern Texas Gulf Coast is retreating at an average rate of about 2.27 m/y.

Bathymetric LIDAR is a fundamental advance in the ability to acquire nearshore data for coastal monitoring and shoreline change studies (Arifin and Kennedy, 2011; Kim, Lee, and Min, 2017; Thatcher *et al.*, 2016; Wozencraft and Lillycrop, 2006; Wozencraft and Millar, 2005; Xhardé, Long, and Forbes, 2011), but the BEG-owned Airborne Hydrography AB (now Leica) Chiroptera airborne mapping system was previously untested under murky-water conditions, which are typical of the Texas coast. The bathymetric data collection portion of this project was the first opportunity to examine the depth capability and water-clarity limitations of the Chiroptera on the open Gulf of Mexico coast. Chiroptera is a shallow-water mapping system (approximately 15 m in optimal water conditions) that is rated as being able to map the subsurface at 1–1.5 times Secchi depth. The Secchi depth, the maximum depth at which a 30-cm-diameter white disk can be seen when lowered into a water body (Preisendorfer, 1986; Tyler, 1968), is used as a guide for determining the depth-measuring capabilities of bathymetric LIDAR systems. The BEG's initial survey to test the bathymetric capabilities of the Chiroptera was a 2012 study on the coastal plain of the Alaskan North Slope that mapped wetland distribution and determined depths and volumes of shallow Artic lakes (Paine *et al.*, 2013, 2015). Water penetration to depths greater than 6 m was achieved in lakes reporting very low turbidities, ranging from 0.7 to 4.3 nephelometric turbidity units (NTU). Turbidity is the concentration of suspended matter in the water column.

Study Area

The study area comprises the southern extent of Padre Island, a long Holocene barrier island that broadens from a narrow peninsula at Brazos Santiago Pass to a broad, sandy barrier island having a well-developed dune system throughout most of its length. A ship channel has been dredged and jetties built at Brazos Santiago Pass, a natural pass that allows tidal exchange between the Gulf of Mexico and Laguna Madre, a shallow lagoon landward of Padre Island. Padre Island is artificially separated into northern and southern segments at Mansfield Channel, a dredged channel protected by short jetties (Kraus, 2007; Morton, 1977). Brazos Island, a coast-parallel spit adjacent to an erosional deltaic headland, lies between Brazos Santiago Pass and the Rio Grande (McGowen, Garner, and Wilkinson, 1977). The Rio Grande created a large fluvial/deltaic headland where it enters the Gulf of Mexico at the U.S.–Mexico border. The Rio Grande has a large drainage basin (471,900 km^2) that extends into Mexico, New Mexico, and Colorado. Dams constructed on the middle and lower parts of

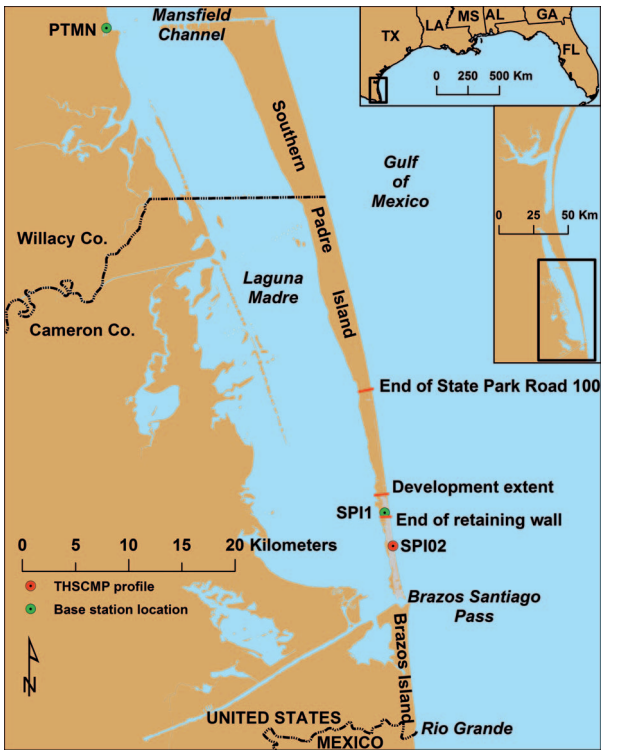

Figure 1. Map of the Texas coastal zone with inset of southern Padre and Brazos Islands (Mansfield Channel to Rio Grande on the U.S.–Mexico border). Developed areas within the City of South Padre Island are indicated.

the basin combined with extensive irrigation use of Rio Grande water on the coastal plain have reduced the amount of sediment delivered to the coast (Brown *et al.*, 1980; Paine, Caudle, and Andrews, 2014).

Prominent geomorphic features on southern Padre Island and Brazos Island include tidal flats, vegetated barrier flats, foredunes, foredune complex, washover channels and fans, sparsely vegetated barrier flats, back-island dunes, and algal flats (Brown *et al.*, 1980; Caudle *et al.*, 2014; McGowen, Garner, and Wilkinson, 1977; Morton and Pieper, 1975). The foredune is a discontinuous, linear, shore-parallel, relatively high-relief feature adjacent to the beach in the fore-island area and includes both stabilized and active dunes. The foredune is the seaward-most line of coastal dunes. Also in the fore-island area, the adjacent foredune complex is composed of relatively low-relief sand dunes and hummocks and is mostly stable, except in disturbed areas. Numerous storm washover channels occur in areas where dunes have little to no vegetation. They become active channels during passage or landfall of tropical cyclones and are closed between storms by sediments transported alongshore (Brown *et al.*, 1980; McGowen, Garner, and Wilkinson, 1977; Morton and Pieper, 1975). In this semiarid climate, the most extensive habitats are broad wind-tidal flats. The wind-tidal flats are developed on sediments transported to the lagoon side of Padre Island by the prevailing southeasterly winds and hurricane washover (Brown *et al.*, 1980).

The Texas Gulf Coast shoreline is microtidal; mean tidal range is 0.4–0.6 m. Vegetation cover is sparse on the southern Texas coast due to a combination of low rainfall and high evapotranspiration rates. This creates an environment of active dunes that offer little resistance to wind or water erosion. The predominant southeasterly winds generate northerly longshore currents. Strong winter northers generate short-lived southward-moving longshore currents (Brown *et al*., 1980).

Southern Padre Island can be divided into four segments based on development intensity (Figure 1). The City of South Padre Island occupies the southernmost portion of the island (10 km) and is highly developed. The developed section of South Padre Island is separated into two sections. A retaining wall limits the landward boundary of the dune complex in the southern 8 km of the city. The northernmost section of the city is an area of recent development that does not have a wall. State Park Road 100 (Padre Boulevard/Ocean Boulevard) continues north for an additional 10 km from the developed portion of southern Padre Island. There has been no development (homes, condominiums, parks, *etc*.) in this segment, but the road provides access to the beach. The road is landward of the dune system, but in areas of active dunes (sparse vegetation), sand has migrated across the road. Occasionally, sand is removed from the road and used for small beach nourishment projects within the city. The northernmost 36 km section of southern Padre Island is undeveloped. Brazos Island is 12 km long and undeveloped.

METHODS

An airborne LIDAR survey conducted by the BEG in 2013 covered a swath along southern Padre Island and Brazos Island that included the beach and adjacent dune complex. LIDAR and associated GPS data were processed to produce point clouds and 1-m-resolution digital elevation models (DEMs) of the ground surface. Shoreline position was determined by extracting a common elevation contour as the shoreline proxy. Shoreline movement was determined for three timescales and compared to historical shoreline change rates determined through 2007. DEMs were used to examine relationships among coastal segments in sediment volume above threshold elevations at 1 m elevation intervals (Paine, Caudle, and Andrews, 2017). Differences in sediment volumes above threshold elevations can reveal differences in sand storage, erosion resilience, and storm flooding susceptibility for the different segments of southern Padre and Brazos Islands.

Principal project tasks included (1) acquiring airborne topographic and bathymetric LIDAR data along southern Padre Island and Brazos Island; (2) processing the topographic and bathymetric LIDAR data to produce full-resolution point clouds and a DEM; (3) extracting a shoreline from the DEM to analyze short- and long-term shoreline change; (4) mapping the landward dune boundary and maximum dune crest; and (5) extracting volume statistics to analyze volumetric change.

Data Acquisition

LIDAR data and color infrared (CIR) aerial imagery of southern Padre Island and Brazos Island, Texas (Mansfield Channel to Rio Grande), were acquired on 4 and 5 February 2013. Data were collected using the BEG's Chiroptera airborne system (Airborne Hydrography AB; now Leica Geosystems, Heerbrugg, Switzerland), which collects topographic LIDAR data, shallow bathymetric LIDAR data, and natural color/CIR imagery. Topographic data and CIR images were collected for a 500 m swath (three passes) of southern Padre Island and Brazos Island (~70 km total length) landward of the shoreline. Bathymetric data were collected from the shoreline 1000 m seaward to establish the depth-penetration and water-clarity limitations of Chiroptera on the open Gulf of Mexico coast. A few transects were also flown across Padre Island and Laguna Madre, capturing both topographic and bathymetric data.

The Chiroptera was installed in a single-engine Cessna Stationaire 206 aircraft (tail number N147TX) owned and operated by the Texas Department of Transportation. Flight elevation was 650 m for the topographic survey and imagery capture of southern Padre Island and Brazos Island. Topographic laser pulse rate was 200 kHz. Flight elevation was 400 m above sea level for the bathymetric survey offshore of southern Padre Island and Brazos Island. The bathymetric laser was operated at the system maximum pulse rate of 36 kHz. Also mounted in the Chiroptera chassis is a Hasselblad DigiCAM 50 megapixel natural color (red-green-blue [RGB]) or CIR camera. CIR aerial images and LIDAR data were collected simultaneously during this survey. GPS and attitude (roll, pitch, and yaw) information was acquired along with LIDAR data and imagery to enable accurate georeferencing. Two GPS base stations, set for continuous 1 second data-collection rate, were operated during the survey at Port Mansfield (PTMN) and the South Padre Island Convention Center (SPI1, Figure 1).

Data Processing

All laser data, raw image files, and positional data were downloaded to a field computer at the end of each survey day. Preliminary field processing occurred daily to examine laser-point-cloud data to determine completeness of the data coverage (*i.e*. sufficient overlap of flight lines and point spacing) and to identify data-quality issues (GPS problems, insufficient data returns, *etc*.).

Topographic LIDAR Postprocessing

Base-station coordinates were computed using the National Geodetic Survey's (NGS) Online Positioning User Service (OPUS). AEROoffice (IGI mbH, Kreuztal, Germany) software was used to extract aircraft GPS data from the Chiroptera's data files and convert it to a binary Novatel GPS file. The aircraft GPS file and base-station GPS files were then converted to a GrafNav-compatible format. A merged aircraft trajectory was computed using Waypoint Software's GrafNav (NovAtel, Inc., Calgary, Alberta, Canada). Solutions for base-station coordinates and aircraft trajectories were output in the North American Datum of 1983 (NAD83). The precise trajectories were combined with aircraft attitude information in AEROoffice to create a final precise seven-parameter (time, X, Y, Z, roll, pitch, yaw) navigation file.

Laser-point cloud data were generated in the processing software Leica LiDAR Survey Studio (LSS, Leica Geosystems, Heerbrugg, Switzerland), combining navigation file information and laser data. The software also requires calibration,

processing settings, and system-configuration files. Laser-point data were output from Leica LSS in LAS v1.2 format (a binary file format) in Universal Transverse Mercator (UTM) Zone 14 coordinates. The resultant points were referenced to the NAD83 horizontal datum and height above the Geodetic Reference System of 1980 (GRS80) ellipsoid. The MicroStation (Bentley Systems, Inc., Exton, Pennsylvania, U.S.A.) TerraScan utility (Terrasolid Products, GeoCue Corporation, Madison, Alabama, U.S.A.) was used to concatenate flight-line segments, combine flight lines, and decimate data into U.S. Geological Survey (USGS) quarter quadrangles, determine bias offsets between LIDAR point data and kinematic GPS ground reference control points, and clean the data of miscellaneous returns (such as clouds, reflections, and long returns).

Kinematic ground GPS surveys of roads and parking lots (open areas with unambiguous surfaces) were conducted within the LIDAR survey area to acquire ground-truth information. The surveyed ground points are estimated to have a vertical accuracy of 0.01–0.05 m. LIDAR data points from the aerial survey were used to generate a DEM with 1 m × 1 m resolution of the area where ground truth information was collected. The ground GPS surveys were superimposed on the DEM and examined for any mismatch between the horizontal position of the ground GPS and the corresponding feature on the DEM. Horizontal agreement between the ground kinematic GPS and the LIDAR was within the resolution of the 1 m × 1 m DEM. The DEM was also compared with aerial photography from the 2012 National Agriculture Imagery Program (NAIP) for horizontal agreement. To determine vertical accuracy, the LIDAR data points were sorted to find data points that fell within 1 m of a ground GPS survey point. The mean elevation difference between the LIDAR and the ground GPS was used to estimate and remove any elevation bias from the LIDAR data. The standard deviation of these elevation differences provides estimates of LIDAR precision. Vertical biases were determined for and removed from each flight. Average root mean square (RMS) vertical error for the 4 February flight is 0.0332 m, and RMS values for the two 5 February flights are 0.0448 m and 0.028 m. The 2012A geoid model (NGS, 2012) was used to adjust the elevation data from ellipsoidal to orthometric heights (NAVD88) using lasheight, a LAStools (rapidlasso GmbH, Gilching, Germany) script. This script was also used to remove elevation bias between the laser-point data and ground-control points. The final DEM was generated from the input LAS files using the LAStools script lasgrid.

Bathymetric LIDAR Postprocessing

The Leica LSS calibration, processing settings, and system-configuration files were updated for bathymetric processing. A calibration file for bathymetric data processing was prepared to align vertical elevation control points with laser point-cloud data and to eliminate roll, pitch, and yaw errors caused by internal measurement unit (IMU) misalignment. The processing settings and configuration files were prepared by setting amplitude thresholds, backscatter threshold values, and a software-computed water-refraction value (based on salinity) to provide optimum processing algorithm performance and minimize noisy data output. Additionally, the "select map" option within Leica LSS was used to automatically determine the water surface elevation from the laser data. After initial processing, waveform information was visually examined to determine if the laser returns were classified properly. After bathymetric laser-point data were output from Leica LSS, the MicroStation TerraScan utility was used to concatenate flight-line segment files, combine adjacent flight lines, and extract Class 7 (bottom/seafloor) and Class 5 (water surface) data as separate files.

Ground truthing of airborne bathymetric data to verify that returns represented the true subsurface bottom was accomplished by comparing data points to reference points based on differential GPS (DGPS), single-beam sonar, multibeam sonar, and multibeam echosounder (MBES) data (Chust *et al.*, 2010; Costa, Battista, and Pittman, 2009; Pastol, 2011; Saylam *et al.*, 2018; Webster *et al.*, 2016; Wright *et al.*, 2016). For this study, offshore single-beam sonar transects collected in October 2012 by Naismith Marine Services, Inc., for HDR Engineering, Inc., the Texas General Land Office, and the City of South Padre Island were used as ground truth for the southern portion of study area. The transect data points were collected within the limits of the City of South Padre Island, a stretch of shoreline 10 km long and extending offshore approximately 1.4 km to water depths between 9 and 10 m. While the sonar data were not collected concurrently with the bathymetric LIDAR survey, the transect data were useful to verify that returns classified by Leica LSS as bottom points were actual seafloor returns.

The 2012A geoid model was used to adjust the elevation data from ellipsoidal to orthometric heights (NAVD88) using the LAStools script lasheight. A bathymetric DEM (3 m cell size) was generated from the input LAS files using the LAStools script lasgrid. The bathymetric grid was then resampled to 1 m spacing, and a smoothing algorithm was run over the new 1 m DEM. The smoothed bathymetric grids were then merged with the topographic grids to create a seamless topographic and bathymetric DEM (Figure 2).

Aerial Imagery Postprocessing

Postprocessing of the imagery used the same GPS and attitude information collected for the LIDAR survey. Hasselblad's Phocus (Gothenburg, Sweden) software was used to export the imagery from its native format to tagged image file (TIF) format. The software also corrected for lens distortion and vignetting. The open source software ImageMagick (https://www.imagemagick.org/) was used to move/reorder channels and then isolate the infrared return to a single channel. The MircoStation utility TerraPhoto was used to orthorectify the images and remove seams between adjacent image frames. The files were exported as 1-m-resolution, 4000 × 4000 m tiles in enhanced compression wavelet (ECW) format. The ECW files were opened in ERDAS ERMapper (Hexagon Geospatial, Stockholm, Sweden), color-balanced, and saved as a single 1 m geoTIF mosaic. The 1 m geoTIF was color-matched in Photoshop (Adobe, San Jose, California, U.S.A.) to existing CIR imagery.

Shoreline Position

Before the advent of LIDAR, vertical aerial photography was commonly used to determine shoreline position. Shorelines were drawn or digitized on the photography by using the

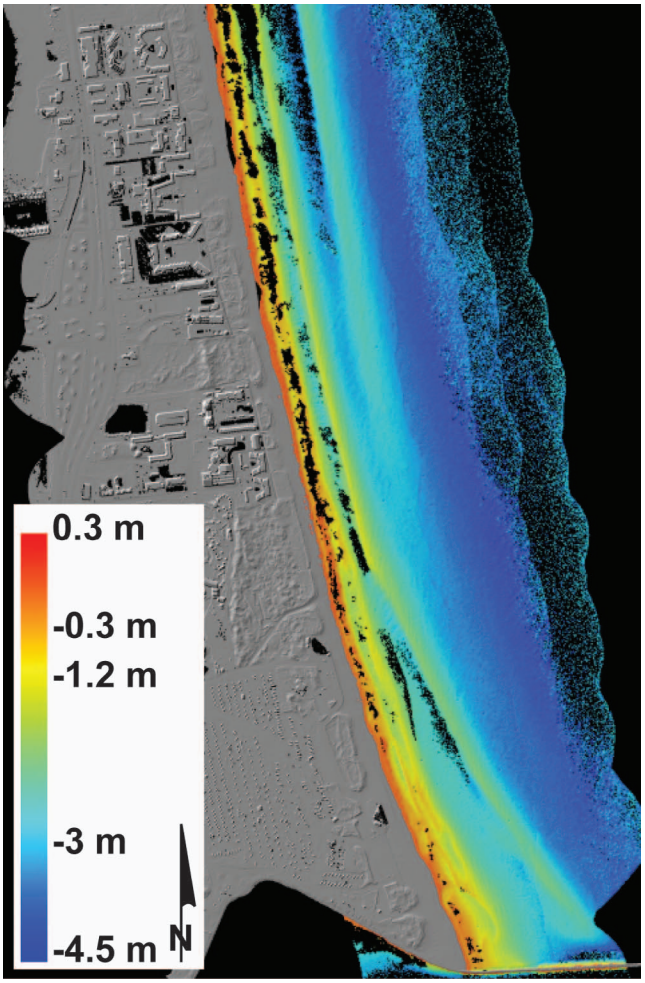

Figure 2. Merged topographic and bathymetric digital elevation model (DEM) for area north of Brazos Santiago Pass. Topographic DEM is illustrated as shaded relief map. Color scale for bathymetric DEM is shown at left (units in meters).

distinct tonal boundary between wet and dry sand on the beach, representing the high water line (HWL). The position of this boundary varied due to water-level conditions, wave activity, and errors in georeferencing the photography. After comparing high-density LIDAR data to traditional ground-based GPS techniques, Sallenger *et al*. (2003) determined that airborne topographic LIDAR data have a vertical accuracy (15 cm) adequate to resolve beach-change signals over large areas for long-term shoreline change analysis. It was also concluded that LIDAR data can be used to investigate impacts of storms, beach recovery following storms, and the natural variation of the shoreline position. LIDAR allows for the rapid collection of high-density data over a large swath of coastline.

Studies have been conducted to determine the best practices for extracting a single elevation contour from LIDAR data to serve as the shoreline proxy. Moore, Ruggiero, and List (2006) suggested that the shoreline proxy needed to be repeatable, consistent from survey to survey, as well as a meaningful indicator of sediment transport on the foreshore. The National Assessment of Coastal Change Hazards Project by the USGS selected the mean high water (MHW) contour, determined using local tide gauges, as the shoreline position (Weber, List, and Morgan, 2005). The datum-based MHW provides a mapping advantage because it is consistent and repeatable, but it falls lower on the beach than the historically used visual HWL interpretation (Moore, Ruggiero, and List, 2006). Stockdon *et al*. (2002) created a statistical approach to rapidly map MHW shoreline position from profiles generated from extremely accurate, high-density LIDAR data. Extracting a MHW or mean higher high water (MHHW) vertical datum from LIDAR data is highly accurate and straightforward.

Selection of a vertical datum that serves as a proxy for a digitized wet/dry line (HWL) is good for historical comparisons but proves difficult to quantify as a precise elevation. Through analysis of LIDAR surveys and repeated beach profiles, Gibeaut and Caudle (2009) and Gibeaut, Gutierrez, and Hepner (2002) determined that the wet beach/dry beach boundary occurred at about 0.6 m above mean sea level (msl) on the Texas Gulf Coast shoreline. The seaward-most, continuous contour of 0.6 m above local msl provided a consistent shoreline feature to serve as a proxy shoreline between LIDAR data sets. Using an elevation that corresponds to the position of the HWL or wet beach/dry beach boundary offers several advantages for shoreline change analysis over using lower tidal elevations, such as msl, MHW, or MHHW: It is comparable to HWL mapped shorelines on historical photography, it is often at an elevation above water level and able to be mapped by LIDAR, and it is above the elevation of high-frequency changes that occur on the lower beachface (*i.e*. swash bar movement or cusp formation) (Gibeaut and Caudle, 2009).

When LIDAR data are processed, the elevation values are reported in height above an ellipsoid (HAE). These values are then transformed to North American Vertical Datum of 1988 (NAVD88) orthometric height by applying a geoid model correction. Previous BEG-acquired LIDAR data sets (2000–12) used the NGS GEOID99 model to make the transformation between ellipsoidal heights and NAVD88 heights. A mean sea-level correction was also applied before extracting the shoreline (0.6 m msl) from the LIDAR data sets. GEOID99 has been superseded by newer geoid models. The NGS produces new geoid models every few years to more accurately represent current surface of Earth and incorporate additional data. The GEOID12A model, released by the NGS in September 2012, was used to transform between ellipsoidal heights and NAVD88 orthometric heights for the 2013 southern Padre Island and Brazos Island shoreline survey. The NAVD88 heights corrected with the GEOID12A model are higher than the heights corrected using the GEOID99 model; therefore, a new shoreline proxy elevation needed to be determined.

To determine the optimal proxy elevation for the 2013 LIDAR-derived shoreline, an analysis was conducted of beach profiles collected by BEG staff and students participating in the Texas High School Coastal Monitoring Program (THSCMP) between 2000 and 2013 (Caudle and Paine, 2017), GPS-based shoreline mapping conducted by THSCMP students near the dates of the LIDAR survey, and observations of the visual wet

beach/dry beach line on aerial photography acquired during the LIDAR survey. THSCMP students used handheld GPS units to map the wet beach/dry beach boundary during their data collection field trips. The 1.05 m above NAVD88 (GEOID12A) contour was selected as the shoreline position proxy for the February 2013 LIDAR DEM through this analysis.

To extract a consistent shoreline proxy from the airborne LIDAR data, the 2013 DEMs were imported into ArcGIS ArcMap (ESRI, Redlands, California, U.S.A.), and the 1.05 m NAVD88 elevation contour was selected using the contour function in ArcGIS. The extracted contour was edited in ArcMap to retain the most seaward, continuous contour and smoothed using a 2 m smoothing tolerance. Topology errors, including dangles, self-overlapping lines, and self-intersecting lines, were removed, and the numbers of vertices in the polyline were reduced using a 0.25 m tolerance, which retained the shape of the smoothed shoreline feature.

Shoreline Change Rates

Long-term shoreline change rates were calculated by including the 2013 southern Padre Island and Brazos Island shoreline into the set of shoreline positions that had been used previously to determine long-term Texas Gulf Coast shoreline change rates presented in the BEG's shoreline change publication series (Morton, 1977; Morton and Paine, 1990; Morton and Pieper, 1975; Paine, Caudle, and Andrews, 2013, 2014, 2017; Paine, Mathew, and Caudle, 2011, 2012; Paine and Morton, 1989). Shoreline positions from the 1930s to 1990 were interpreted by mapping the wet beach/dry beach boundary from vertical aerial photographs, which was then optically transferred to USGS 7.5 minute paper topographic base maps. These shoreline positions were digitized from the paper maps into an ArcGIS format. The 1995 shoreline was digitized as the wet/dry boundary directly from orthorectified digital aerial imagery. Shoreline proxy positions (0.6 m above msl, corrected using Geoid99 model) from 2000, 2010, 2011, and 2012 were extracted from LIDAR-derived DEMs created from LIDAR surveys conducted by using the BEG's Optech ALTM 1225 instrument. The 2013 shoreline position was extracted from the LIDAR-derived DEM at 1.05 m above NAVD88 (Geoid12A).

Shorelines selected for this change rate analysis corresponded to shorelines chosen during previous shoreline change rate studies in the study area. The shorelines were also selected to give reasonably regular time intervals between shorelines along a given transect. The included shorelines for the long-term change rate calculation were from 1937, 1960, 1974, 1975, 1995, 2000, and 2013. One approach that can be used to assess whether shoreline movement rates were increasing, decreasing, or remaining constant over time is to compare long-term rates with rates measured over shorter and more recent periods. Shoreline positions (elevation contour used as the shoreline proxy) from airborne LIDAR surveys conducted in 2000, 2010, 2011, 2012, and 2013 were included for a decadal-scale and short-term shoreline change analysis.

Shoreline movement between the different time periods (long-term 1937–2013, decadal 2000–13, and short-term 2010–13) was measured along shore-normal transects spaced at 50 m intervals along the southern Padre Island and Brazos Island shoreline using the Digital Shoreline Analysis System (DSAS) within ArcGIS (Thieler *et al.*, 2009). The DSAS extension was then used to calculate rates of change and associated statistics using the transect location and the selected shorelines. Change rates were calculated as both linear regression rate (best-fit movement rate for all shoreline positions using a least-squares regression line) and net (or endpoint) rates (net movement rate between the oldest and youngest shoreline position).

Potential Vegetation Line

Mapping the natural line of vegetation has proven difficult when establishing a legal boundary for the Texas Open Beaches Act (OBA). The OBA defines the landward boundary of the public beach easement as the line of vegetation indicated by "the extreme seaward boundary of natural vegetation which spreads continuously inland" (Texas Natural Resource Code, 1991). Gibeaut and Caudle (2009) sought to establish a consistent mapping technique based upon LIDAR elevation data that could be used to determine the "potential vegetation line" or PVL. Because of the difficulty in rigorously mapping the landward boundary of the public beach easement as the line of vegetation due to variation in vegetation density along the Texas coast, vegetation line retreat due to storm impacts, different rates of natural poststorm recovery, and human manipulation, Gibeaut and Caudle (2009) recommended that an elevation be selected that represents the lowest elevation at which foredune vegetation may potentially form a natural continuous cover. The seaward-most contour line with an elevation of 1.50 m above NAVD88 (GEOID12A) was used as the boundary or PVL proxy elevation. This elevation was derived from statistical analysis of long-term (1999–2013) beach profile elevation data of natural dunes along the south Texas coast. The extracted PVL proxy elevation will either be within the vegetation or coincide with the vegetation line. Where the PVL lies seaward of the vegetation, it indicates the potential position to which vegetation and the foredune may advance.

To extract a consistent PVL, the 2013 DEMs were imported into an ESRI ArcMap project, and the 1.5 m NAVD88 (GEOID12A) elevation contour was selected using the contour function. The relatively continuous contour line along the back edge of the beach and seaward edge of the foredune was selected as the PVL. The extracted contour was edited in ArcMap to retain a continuous contour line along the back edge of the beach and seaward edge of the foredune and smoothed using a 2 m smoothing tolerance. Topology errors (including dangles, self-overlapping lines, and self-intersecting line) were removed, the number of vertices in the polyline were reduced using a 0.25 m tolerance which retains the shape of the smoothed feature, and adjacent line segments were aggregated to create the final GIS shapefile.

Landward Dune Boundary

The position of the landward dune boundary is an important factor in determining the space required for dune formation, defining the foredune complex for volumetric and geomorphic analysis, and for use in determining design setback distances or creating dune restoration projects. An automated process for selecting the boundary is not effective because the landward dune boundary is based upon qualitative criteria that are interpreted by examining a combination of LIDAR data and

aerial photography. Several criteria influence the selected position of the landward dune boundary. The boundary should (1) be at or near a change in slope from steep on the dune (>10%) to gentle on the barrier flat (<10%); (2) have an elevation 2 m or more above NAVD88; (3) bound dunes that provide at least minimal storm-surge protection; (4) have an orientation that roughly parallels the shoreline; (5) be adjacent to the shoreline and features classified as dunes; and (6) connect adjacent forms classified as dunes (Gibeaut and Caudle, 2009).

The landward dune boundary for the study area was manually digitized at scales of 1:1000 to 1:5000 using the February 2013 DEMs imported into ArcMap. The foredune complex was defined as the seaward-most continuous feature with an elevation of at least 2 m above NAVD88. If a single continuous feature was not present, dune clusters were considered as part of the complex as long as they were arranged quasi-parallel to the shore and were close together or connected. In areas where dunes were not present (washover areas), the dune boundary was mapped as the landward contour equivalent to the height of the potential vegetation line (1.5 m NAVD88). A GIS-generated raster file representing the aspect of the DEM was used to help interpret the extent of the dune boundary by visualizing the landward slope of dune features. In addition, aerial imagery was used to locate the extent of vegetation and to help identify man-made structures. Man-made structures are not considered to be part of the foredune complex; therefore, the landward dune boundary was placed seaward of buildings or retaining walls.

Maximum Dune Crest Position and Volume Statistics

Evaluating the maximum dune crest height and the volume of sediment in the beach and dune system helps scientists and decision makers understand beach and dune morphodynamics, analyze storm impacts, assess hurricane inundation vulnerability, and appraise alongshore foredune variation (Houser, Hapke, and Hamilton, 2008; Houser and Mathew, 2011; Revell, Komar, and Sallenger, 2002; Stockdon, Doran, and Sallenger, 2009; Woolard and Colby, 2002). Manual digitization of the position of the foredune crest is both time-consuming and subject to an individual's interpretation of a DEM. The highest dune crest elevation (over 2 m) was extracted along transects perpendicular to the southern Padre Island and Brazos Island shoreline, using a spacing of 5 m. A C++ command-line executable program (Shorestat.exe) was written at the BEG to open a DEM and the shoreline file to extract this information. Shorestat also simultaneously calculated sand volume (m^3/m) in the beach and dune system along each transect.

The 2013 shoreline and landward dune line shapefiles for southern Padre Island and Brazos Island were merged and converted into a polygon file. The polygon file was then used to clip the full data set DEM. This step creates a data set that represents the beach and dune system only. The shoreline shapefile was exported to create an ASCII text file containing the horizontal position of the shoreline. Shorestat opened the clipped DEM and the shoreline text file to extract the dune crest position and height as well as the sand volume in the beach and dune system.

Using the shoreline text file, shorestat was used to generate a pseudo-shoreline *x*-*y* coordinate set along the 2013 shoreline elevation at 5 m spacing. Transects perpendicular to the 2013 shoreline file would complicate dune crest extraction and volume calculations, because, in many places, adjacent transects would not be sufficiently parallel to each other; therefore, a pseudo-shoreline was generated by shorestat by averaging the shoreline deviation from true north up and down the coast and then generating new points at 5 m intervals using the nearest average angle deviation from true north.

Shorestat calculated shore-perpendicular transects using the deviation angle plus 90 degrees at each pseudo-shoreline coordinate. The program traversed each transect at 1 m intervals, (1) seeking the highest point along transect, and (2) calculating sand volumes at each 1-m-interval location. Shorestat extracted all the *z*-values from the DEM along each transect, selecting the highest elevation point along with its *x*-*y* position. Sand volume was calculated above six threshold elevations starting at 1 m above NAVD88. Volume was also presented as a percentage of total sand above each elevation threshold. All of the sand in the beach and dune system is above 1 m NAVD88; therefore, that column represents 100%. After completion of the calculations, Shorestat created output text files that record dune crest location and elevation and sediment volume statistics above each elevation threshold at each transect. The text files were then loaded into Global Mapper and exported to ArcGIS shapefile format with an accompanying database.

RESULTS

Critical coastal features were extracted from high-resolution DEMs constructed from the 2013 survey of southern Padre Island and Brazos Island. The 2013 shoreline position was compared to previously mapped shoreline positions to determine shoreline change on historical, decadal, and short-term timescales. Beach and dune volumes above threshold elevations (1 to 6 m) were extracted from the DEMs to assess sand storage on the southern Texas Gulf Coast. The bathymetric data collected using Chiroptera were analyzed to examine the depth limitations of the system in turbid water.

Shoreline Change

Shoreline change rates were determined from three different timescales; long-term 1937–2013, decadal 2000–13, and short-term 2010–13. Historical shoreline positions were determined from the mapping of the wet beach/dry beach boundary on aerial photographs. The 2000 and 2010–13 shoreline positions were extracted from LIDAR DEMs as a standard elevation contour selected as the shoreline proxy.

Long-Term Change, 1937–2013

Rates of long-term gulf shoreline change for southern Padre Island and Brazos Island, calculated from multiple shoreline positions between 1937 and 2013 (Figure 3), averaged 2.2 m/y of retreat for both net rate and linear regression rate calculations. Rates were calculated at 1343 sites spaced at 50 m between Mansfield Channel and the Rio Grande. Net retreat occurred at 1149 sites (86%), and advance occurred at 194 sites (14%) over the period of record. The overall rate is comparable

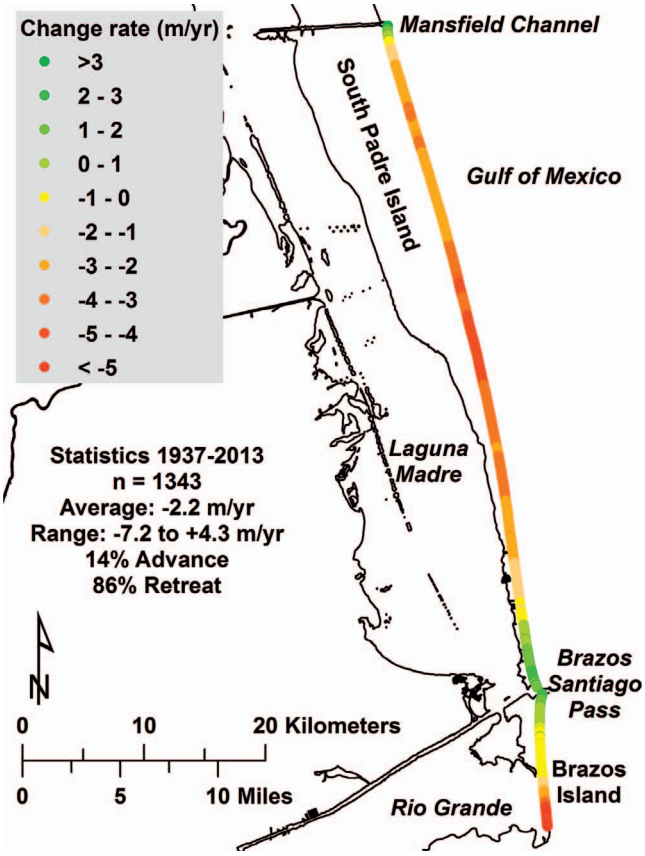

Figure 3. Net rates of long-term change for southern Padre Island and Brazos Island calculated from shoreline positions from 1937 through 2013.

to the average change rate determined from the most recent BEG updates (Paine, Caudle, and Andrews, 2013, 2014, 2017; Paine, Mathew, and Caudle, 2011, 2012).

Net change rates at individual sites ranged from advance at 4.3 m/y to retreat at 7.2 m/y. Net advancing shorelines included a 5.4 km segment adjacent to the north jetty at Brazos Santiago Pass, a 3 km segment adjacent to the south jetty at Brazos Santiago Pass, and a 1.3 km segment adjacent to the south jetty at Mansfield Channel (Figure 3). Net retreating shorelines included 49 km of southern Padre Island and an 8 km segment north of the Rio Grande (Figure 3). The highest net rates of shoreline retreat (greater than 3 m/y) occurred along a 22 km segment in the middle of southern Padre Island and a 2 km segment just north of the Rio Grande.

Brazos Island, between Brazos Santiago Pass and the Rio Grande, had an average net shoreline change rate of 1.2 m/y of retreat (Table 1). Retreat was occurring at 72% of sites on Brazos Island. The highest rates of retreat (7.2 m/y) were found on Brazos Island in a small segment adjacent to the Rio Grande. The area protected by a retaining wall within the developed portion on southern Padre Island experienced the least amount of average net shoreline change within the entire study area. The shoreline in this segment advanced at an average rate of 0.6 m/y. The shoreline advanced at 67% of the sites along the retaining wall. The undeveloped area of southern Padre Island underwent the highest average retreat rates 3 m/y (Table 1). Less than 1% of the sites in the undeveloped area of southern Padre Island were advancing. The highest rate of shoreline advance (4.4 m/y) was measured adjacent to the jetty at Mansfield Channel.

Decadal Change, 2000–13

Rates of decadal-scale gulf shoreline change for southern Padre Island and Brazos Island, calculated from LIDAR-derived shoreline positions from 2000 and 2010–13 (Figure 4), averaged 1.1 and 1.3 m/y of retreat for net rate and linear regression rate calculations, respectively. Rates were calculated at 1340 sites spaced at 50 m between Mansfield Channel and the Rio Grande. Net retreat occurred at 1018 sites (76%), and advance occurred at 322 sites (24%) over the period (Figure 4). The overall rate was 1 m/y less than the long-term rate of change calculated (Table 1).

Net change rates at individual sites ranged from advance at 2.7 m/y to retreat at 6.1 m/y. Net advancing shorelines included a 1.4 km segment adjacent to the north jetty at Brazos Santiago Pass, a 5 km segment adjacent to the south jetty at Brazos Santiago Pass, and a 6.5 km segment within the developed area (with retaining wall) on southern Padre Island. Net retreating shorelines included a 6 km segment north of the Rio Grande and most of the undeveloped shoreline on southern Padre Island (Figure 4).

Brazos Island had an average net shoreline change rate of 0.3 m/y of retreat (Table 1). Retreat occurred at 56% of sites on Brazos Island. The developed area of southern Padre Island, including the retaining wall, experienced the lowest average net shoreline change rates within the entire study area. The shoreline in these segments advanced at a net average rate of 1.1 m/r (no retaining wall) and 0.7 m/y (with retaining wall). The shoreline advanced at 82% of the sites within the City of

Table 1. *Comparison of historical (1937–2013) and decadal (2000–13) shoreline change rates for southern Padre Island and Brazos Island.*

	Historical Rates 1937–2013			Decadal Rates 2000–13		
Study Area	No.	Net Rate (m/y)	Linear Regression Rate (m/y)	No.	Net Rate (m/y)	Linear Regression Rate (m/y)
Whole study area	1343	−2.2	−2.2	1340	−1.1	−1.3
Southern Padre Island (56 km)	1122	−2.4	−2.5	1120	−1.3	−1.4
Undeveloped (36 km)	720	−3.0	−3.1	719	−1.7	−2.0
Undeveloped w/ road (10 km)	208	−2.8	−3.0	207	−1.6	−1.7
Developed w/o wall (2 km)	33	−1.4	−1.4	33	1.1	0.9
Developed w/ wall (8 km)	161	0.6	0.7	161	0.7	0.8
Brazos Island (11 km)	221	−1.2	−1.1	220	−0.3	−0.5

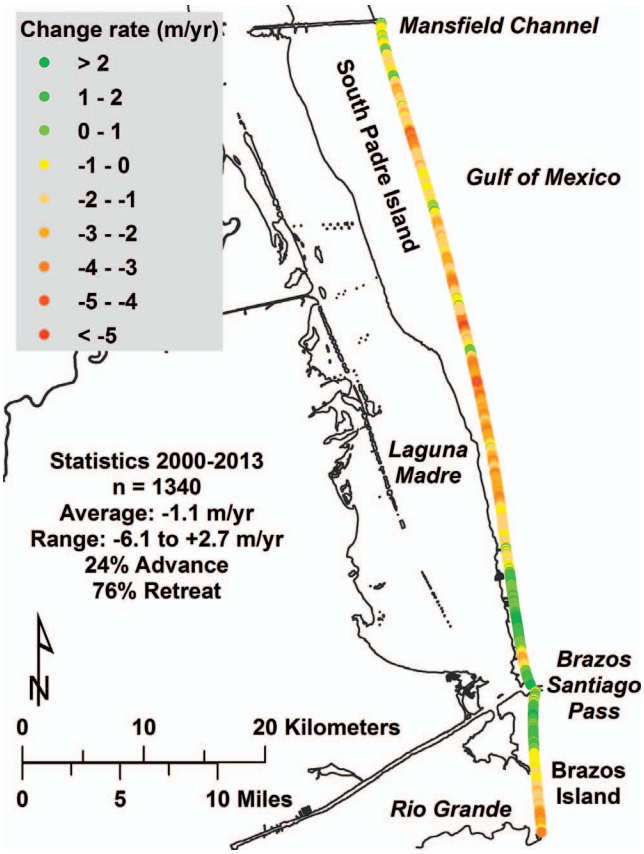

Figure 4. Net rates of decade-scale change for southern Padre Island and Brazos Island calculated from LIDAR-derived shoreline positions from 2000 and 2013.

South Padre Island. The undeveloped area of southern Padre Island (with and without State Park Road 100) underwent the highest average retreat rates of 1.7 m/y (Table 1). The shoreline at 93% of the undeveloped sites was retreating during this time period. The highest rates of shoreline retreat (up to 6 m/y) were in the undeveloped section of southern Padre Island near the midpoint between Mansfield Channel and Brazos Santiago Pass (Figure 4).

Short-Term Change, 2010–13

Short-term shoreline change was determined from annual airborne LIDAR surveys in April 2010, April 2011, February 2012, and February 2013. Rates of change can be misleading over a short period of time (3 years); therefore, change is presented as a distance rather than a rate. The southern Padre Island and Brazos Island shoreline predominantly advanced between the annual airborne LIDAR surveys (Figure 5). Change measured along the coast was positive (advancing) at 64% of the 1342 measurement sites between Mansfield Channel and the Rio Grande; the average distance that the shoreline advanced was 4.9 m (Figure 5; Table 2).

Varying amounts of shoreline change were measured along the study area (Figure 5; Table 2). The greatest amounts of net shoreline advance, more than 30 m, were found adjacent to the

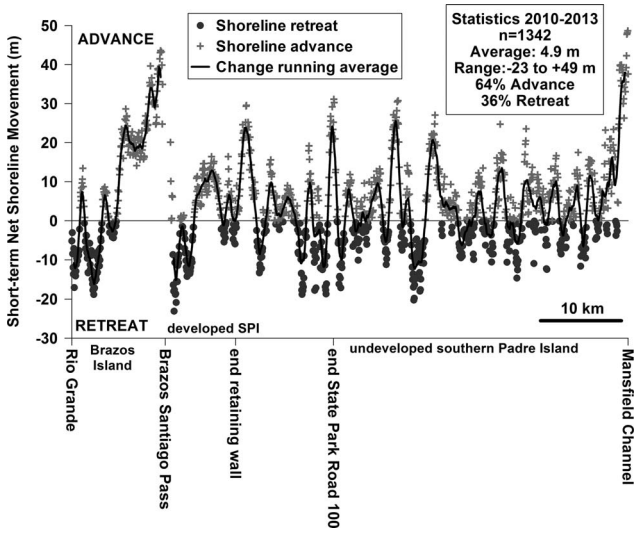

Figure 5. Short-term shoreline change between Rio Grande and Mansfield Channel showing alongshore fluctuations between advance and retreat. Points are spaced every 50 m alongshore, with crosses representing advance and circles representing retreat. Solid line is running average encompassing 11 data points or 500 m of shoreline. The running average illuminates the alongshore fluctuations between advancing and retreating shorelines during this short study period (2010–13).

south jetties at both Mansfield Channel and Brazos Santiago Pass. Shoreline retreat of more than 10 m occurred at 9% of the monitoring locations scattered throughout the study area. The new development area without a retaining wall had the greatest average net shoreline advance of 15.5 m (range –2 to 30 m). The segment with the lowest net shoreline advance was the developed area of southern Padre Island with the retaining wall (Table 2).

Monitoring sites where the shoreline advanced (crosses, Figure 5) between 2010 and 2013 and sites where the shoreline retreated (circles, Figure 5) showed no obvious pattern or trend in the movement of the shoreline. A running average fit line was added to the data points to assist in interpreting the shoreline movement. The running average fit was generated by taking the average of the data within a specified range on either side of a given point. A window width of 11 points was used to generate the running average, including 5 points (250 m) on either side of a given data point. The average was then plotted as a fit line that connects all the average points. The running average line in Figure 5 helps to illustrate the pattern

Table 2. *Net shoreline change determined from shoreline position extracted from airborne LIDAR data acquired in April 2010 and February 2013.*

Area	No.	Net Change (m)	Std. Dev. (m)	Range (m)
Whole study area	1342	4.9	12.0	–23 to 49
Southern Padre Island	1122	4.0	10.7	–23 to 49
Undeveloped	720	4.6	10.8	–20 to 49
Undeveloped w/ road	208	1.7	9.9	–19 to 29
Developed w/o wall	33	15.5	9.6	–2 to 30
Developed w/ wall	161	1.5	9.3	–23 to 20
Brazos Island	220	9.8	16.4	–19 to 43

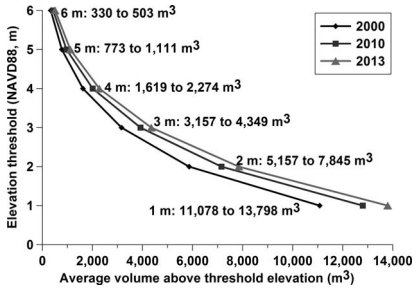

Figure 6. Average volume of sand above NAVD88 threshold elevations in 2000, 2010, and 2013 for the entire study area. Threshold volume increased through time.

of alongshore fluctuations between shoreline retreat and advance during this short study period.

Volumetric Analysis

The DEM created by this study provides a wealth of information about the beach and dune system of southern Padre and Brazos Islands. The DEM was sliced at multiple elevation thresholds to examine the volume of sediment in the beach and dune system. A program was written (Shorestat) to calculate the total volume of sand stored above the 1 m elevation threshold in the beach and dune system. The beach and dune system was defined as the area falling landward of the extracted shoreline and seaward of the mapped landward dune boundary. Volumes were also calculated above the 2 m elevation threshold through 6 m elevation thresholds. Examining the volume of sediment stored above threshold elevations in the beach and dune system can be helpful for understanding several important characteristics related to coastal geomorphology. These include (1) susceptibility to storm surge and flooding at differing surge heights, (2) sand storage within the beach and dune system, and (3) resistance and recoverability from chronic and instantaneous erosion events. Extraction of volume information from previous LIDAR surveys also provides a means to monitor volume change over time.

Volumetric analyses of the beach and dune system on southern Padre Island and Brazos Island are important for understanding current sand storage of the environment and characterized the areas that are more susceptible to storm surge of varying levels. Volume statistics were calculated for the beach and dune system within the study area from three LIDAR surveys: August 2000, April 2010, and February 2013 (Figure 6; Table 3). Plots of threshold elevation against average volume exceeding that elevation for each time period reveal a rapid reduction in volume of sediment as threshold elevations are increased. For example, at the 3 m elevation, the dune contains 3157 m^3 (2000) to 4349 m^3 (2013) of sand at or above that elevation. Above the 4 m threshold, a little more than half that volume of sand (1619 m^3 in 2000 to 2274 m^3 in 2013) is at or above that elevation. The reduction of volume by approximately half with each 1 m increase in threshold elevation is constant throughout the 1 to 6 m elevation ranges, similar to the relationship noted for the entire Texas Gulf Coast shoreline (Paine, Caudle, and Andrews, 2017). Both Figure 6 and Table 3 show that beach and dune system volume in the study area has steadily increased at each threshold elevation since 2000. Plots of volume above different threshold elevations were constructed for both Brazos and southern Padre Islands (Figure 7a) as well as for the different southern Padre Island segments examined in the shoreline change analysis (Figure 7b). The volume statistics represented in Figure 7 were calculated from the 2013 LIDAR data.

Table 3. *Total combined volume of sand above threshold elevations in beach and dune system on southern Padre Island and Brazos Island.*

Threshold Elevation (m)	Total Volume (m^3)		
	2000	2010	2013
6	444,477	571,654	676,397
5	1,039,879	1,293,325	1,495,931
4	2,178,777	2,700,680	3,060,326
3	4,249,298	5,270,829	5,853,264
2	7,893,530	9,629,415	10,559,058
1	14,910,923	17,232,382	18,572,063

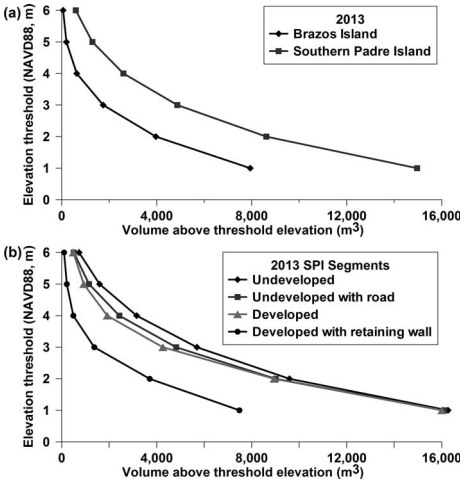

Figure 7. Average volume of sand above NAVD88 threshold elevations for (a) southern Padre Island and Brazos Island and (b) southern Padre Island segments calculated from 2013 LIDAR-derived DEMs.

Much less sand is stored in the beach and dune system on Brazos Island than on the whole of southern Padre Island (Figure 7a). This is due to a generally narrower beach and dune system on Brazos Island. The trend of the volume above threshold elevations on Brazos Island is very similar to the curve from the sites within the developed portion of southern Padre Island that is backed by the retaining wall. The width of the beach and dune system within this developed section of southern Padre Island is limited, owing to the retaining wall serving as the fixed landward dune boundary. The developed segment of southern Padre Island contains few areas with sand storage and dune crests greater than 4 m (Figure 8). A small area near the southernmost point of southern Padre Island (adjacent to Isla Blanca Park) has a wide and well-vegetated foredune complex with dune crests greater than 6 m.

Figure 8. Example of area in developed segment with retaining wall of southern Padre Island showing (a) maximum dune crest elevations and areas of threshold elevations greater than (b) 2 m, (c) 4 m, and (d) 6 m NAVD88. Note there are no areas greater than 6 m in the beach and dune system.

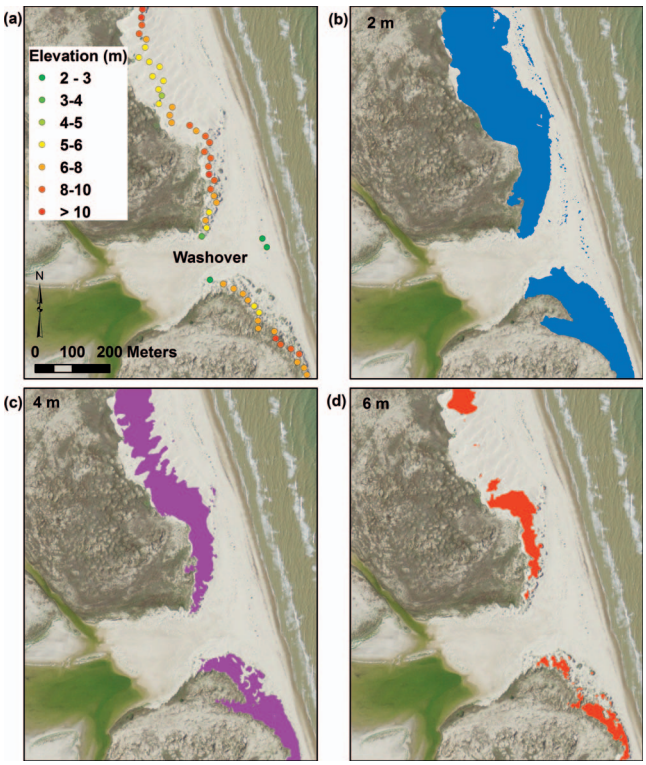

Figure 9. Example of area in undeveloped segment of southern Padre Island showing (a) maximum dune crest elevations and areas of threshold elevations greater than (b) 2 m, (c) 4 m, and (d) 6 m NAVD88. Elevation within the washover feature is 1.2 to 2 m above NAVD88.

The undeveloped areas of southern Padre Island have an extensive foredune complex, except for areas of washover features (Figure 9). Storage capacity within the undeveloped sections (with and without the road) is high, owing to the lack of anthropogenic influences constraining the dune system. The volume of sand at the higher elevation thresholds is slightly lower for the undeveloped area with State Park Road 100 than for the segment without the road (Figure 7), probably as a result of maintenance removal of sand to keep the road clear. The small developed segment without a retaining wall contains significantly more sand, particularly at the lower threshold elevations, than the segment with the retaining wall. The volume trend more closely mimics what is observed in the undeveloped areas.

Bathymetric LIDAR Assessment

The bathymetric LIDAR acquired in February 2013 was compared to data obtained from 53 single-beam sonar lines collected offshore of the City of South Padre Island by Naismith Marine Services, Inc., in October 2012. Turbidity and Secchi depth measurements were not conducted at the time of the LIDAR survey; therefore, the sonar data proved highly beneficial for ground truthing the LIDAR returns within the study area despite the time elapsed between the two surveys. The southernmost sonar transect was used to verify that actual seafloor returns were captured in the area adjacent to the north jetty at Brazos Santiago Pass (Figure 10). The protected waters in this area were sufficiently clear (less sediment suspended in the water column at the time of the survey) to allow the bathymetric laser to penetrate the water column. Returns classified by Leica LSS software as "bottom" in this small part of the study area were considered reliable depth measurements when compared with the sonar data. The LIDAR data points (circles in Figure 10) illustrate a smooth seafloor surface at depths similar to the sonar data points (crosses in Figure 10). A maximum seafloor depth of 4 m was detected by the bathymetric LIDAR. Differences in nearshore bars were expected due to the time elapsed between the surveys (October 2012 to February 2013) as well as a beach nourishment project that took place between November and December 2012 (Perry, 2013, 2014). A second area of true seafloor returns was detected adjacent to the north jetty of Mansfield Channel.

Water conditions, specifically wave activity in the surf zone and water clarity, in the majority of the study area were not ideal for the Chiroptera green laser to penetrate the water column. LSS-classified "bottom" returns in these areas were reflections within the water column, not true seafloor returns. A strong subsurface return signal should have two distinctive peaks in the waveform (Figure 11a)—the first from the water's surface and the second from the bottom surface (seafloor),

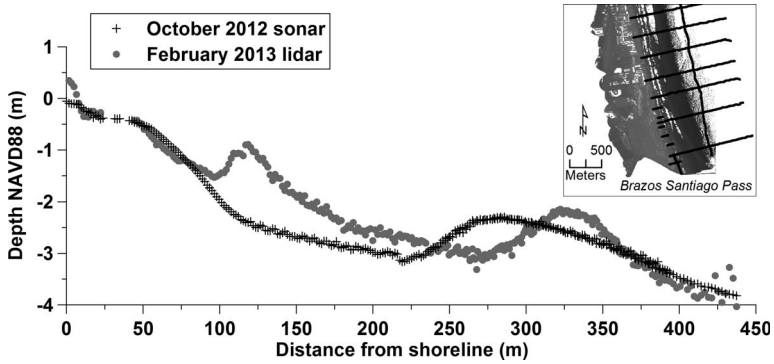

Figure 10. Comparison of February 2013 bathymetric LIDAR data with October 2012 single-beam sonar. Data points are from southernmost transect line near the north jetty of Brazos Santiago Pass (see inset LIDAR image for location).

where the laser is reflected back to the receiver. Noisy waveforms will have indistinct or multiple smaller return peaks (arrows in Figure 11b) as a result of scattering off of sediment suspended in the water column. With further analysis of the bathymetric waveforms and enhanced Leica LSS algorithms, additional seafloor returns may be extracted from the data in this and other coastal areas with less-than-ideal water conditions. This is an area of active research at the BEG and Leica, where algorithms are under development that are expected to improve characterization of true seafloor returns and minimize misclassification of water-column returns. Optimally, future bathymetric LIDAR surveys of the Texas coast should include concurrent sonar or other bathymetric ground truth at multiple locations within the survey area to aid in the validation of water-bottom returns (Saylam *et al.*, 2018). Turbidity and Secchi depth measurements provide vital information to determine when water-clarity conditions are suitable for obtaining optimal bathymetric LIDAR surveying results within the study area.

DISCUSSION

Between 1997 and 2012, the U.S. Army Corps of Engineers (USACE) completed 13 beneficial use of dredged material (BUDM) projects using sediment dredged from Brazos Santiago Pass (Table 4; Perry, 2013, 2014). Sediment was either placed directly onto select beaches in the City of South Padre Island (nourishment) or in a nearshore berm (water depth approximately 9.8 m). Three of the projects (in 1997, 1999, and 2002) placed sand both as nourishment and in a nearshore berm. The projects in 2003, 2006, 2007, and 2008 placed sediment into nearshore berms. The projects in 2000, 2005, 2009, 2010, 2011, and 2012 were beach nourishment projects. The 2010 and 2011 LIDAR surveys were both flown in early April, which occurred after the beach nourishment projects during those years (February–March time frame). The 2012 beach nourishment occurred during November and December, between the February 2012 and February 2013 LIDAR surveys, and also between the October 2012 single-beam sonar survey and the February 2013 bathymetric LIDAR survey.

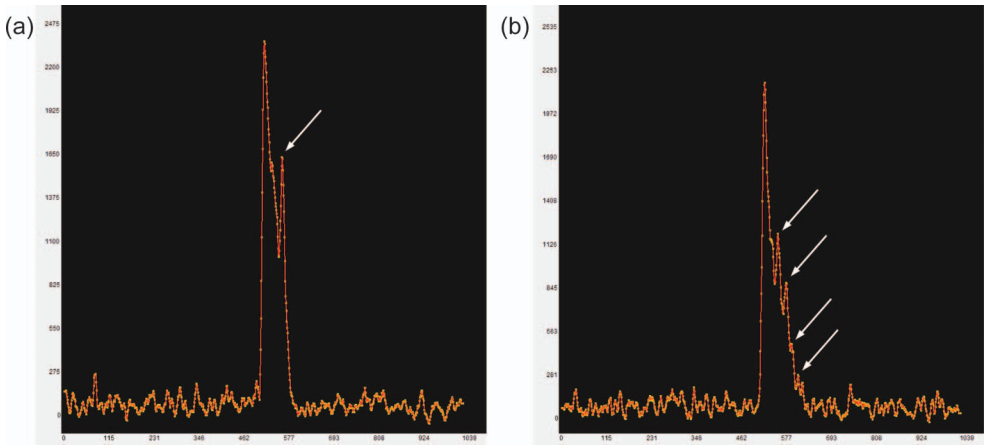

Figure 11. Comparison of waveform returns in (a) clear water with two strong peaks representing the water surface and seafloor (arrow) and (b) a noisy waveform pattern in murky water. The first distinct peak represents the water surface. The multiple smaller peaks that follow (arrows) represent a scattering of the laser pulse owing to sediment in the water column.

Table 4. *Southern Padre Island dredged material placement history (Perry, 2013, 2014).*

Year	Type of Placement	Estimated Dredged Volume (yd^3)	(m^3)
1997	Nourishment	490,000	374,850
	Nearshore berm	396,000	302,940
1999	Nourishment	495,000	378,675
	Nearshore berm	195,000	149,175
2000	Nourishment	370,000	283,050
2002	Nourishment	330,000	252,450
	Nearshore berm	329,000	251,685
2003	Nearshore berm	356,000	272,340
2005	Nourishment	278,000	212,670
2006	Nearshore berm	340,000	260,100
2007	Nearshore berm	443,000	338,895
2008	Nearshore berm	500,000	382,500
2009	Nourishment	407,000	311,355
2010	Nourishment	220,000	168,300
2011	Nourishment	567,000	433,755
2012	Nourishment	350,000	267,750

The BUDM projects are likely one factor responsible for the difference between the lower (less negative) decadal shoreline change rate of –1.1 m/y and the historical rate of –2.2 m/y, as well as the average shoreline advancement documented between 2010 and 2013 (Figure 5). Figure 12 compares the long-term shoreline change rates at the monitoring sites in the study area with the decadal-scale (2000–13) change rates and the short-term (2010–13) shoreline movement. The trend of the decade-scale change rates mimics the long-term trends along the length of the study area, except that the decade-scale rates are generally higher on the graph (lower retreat, higher advancement rates). A notable exception is adjacent to the south jetty at Mansfield Channel, where the highest rates of shoreline advancement are recorded in the long-term record, whereas between 2000 and 2013, the shoreline was retreating (~1 m/y) or stable. Fluctuations also exist in the decadal-scale

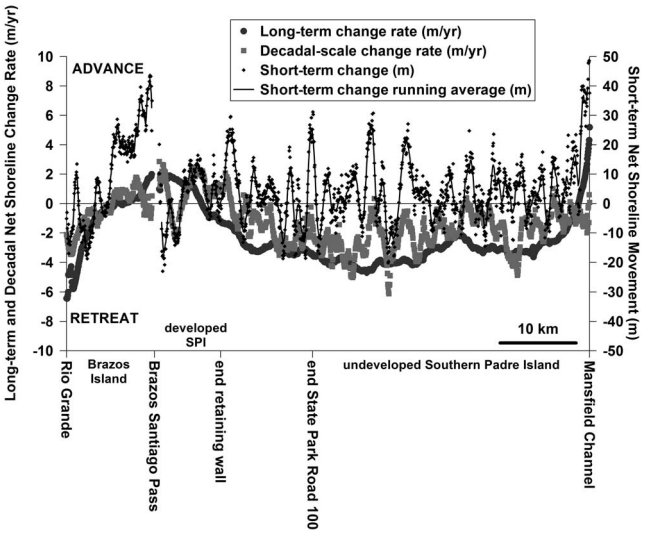

Figure 12. Comparison of historical and decadal-scale net shoreline change rates (m/y) with short-term net shoreline movement (m).

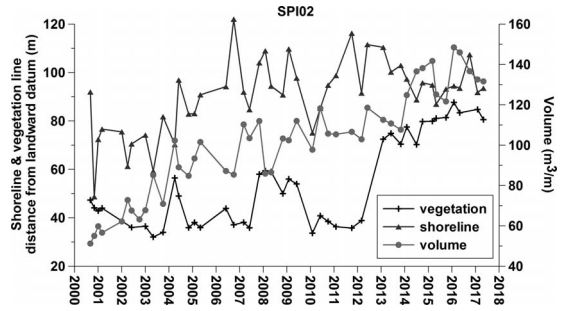

Figure 13. Changes in shoreline position, vegetation line position, and sediment volume at SPI02 (Moonlight Circle, Beach Access 13) within the City of South Padre Island as measured by Port Isabel High School students participating in the Texas High School Coastal Monitoring Program between 2000 and 2017.

shoreline change rates alongshore, which are generally smoothed throughout the long-term rates. This trend mimics the fluctuations between advancement and retreat noted in the short-term shoreline change. The movement of the shoreline in the short-term and decadal-scale monitoring periods could represent the redistribution of sediments from the BUDM beach nourishment projects that have taken place since 1997.

The advance and retreat of shorelines following nourishment projects within the developed portion of southern Padre Island have been documented by students participating in the THSCMP at all three of their sites (Caudle, 2017; Caudle and Paine, 2012, 2017; Caudle *et al*., 2014). SPI02 is a THSCMP beach monitoring site located at Beach Access 13 (Moonlight Circle), approximately 4.5 km north of Brazos Santiago Pass, or the midpoint of the developed area with the retaining wall on southern Padre Island (Figure 1). Port Isabel High School students have been monitoring an overall trend of shoreline advancement and sediment volume increase throughout their study period (2000–17; Figure 13). The advancement of the shoreline and increase in sediment volume are results of the combination of beach nourishment, dune restoration (sand fences and vegetation planting), and beach maintenance practices at this study site. The beach maintenance practiced on a limited basis within the City of South Padre Island involves beach scraping to remove excessive seaweed. The sand and seaweed scraped from the beach are placed just seaward of the vegetation line, creating a "push-up" or man-made dune.

Rapid changes in the nearshore environment occurred between the October 2012 single-beam sonar data collection and the February 2013 bathymetric LIDAR survey. An offshore bar (crest height 0.5 m) formed within 125 m of the shoreline in water 1.5 m deep (Figure 10). This offshore bar may have formed due to redistribution of sediment following the beach nourishment project that took place in November and December 2012. Nearshore bars have been found to form rapidly after beach construction as part of typical postnourishment profile equilibrium (Roberts and Wang, 2012). Other studies monitoring the nearshore environment have documented bars that form and migrate seasonally (Brutsché *et al*., 2014; Houser and Barrett, 2010; Ruggiero *et al*., 2009; Williams and Kraus, 2011)

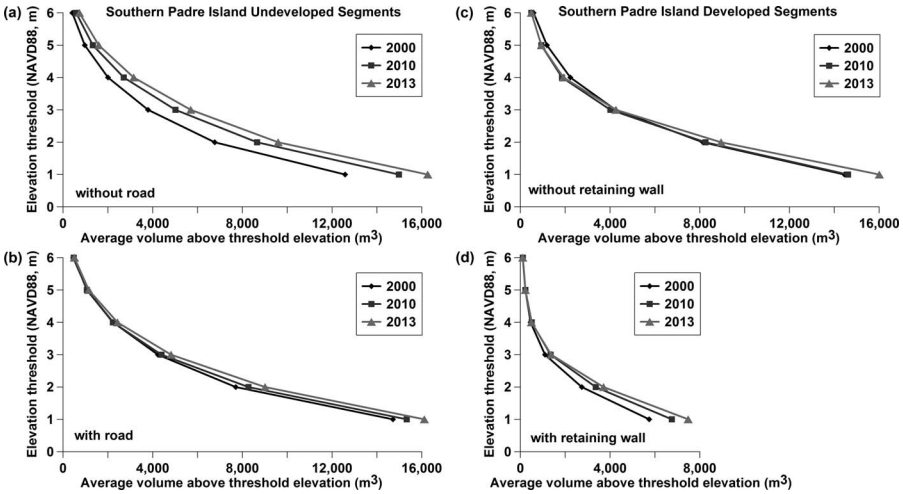

Figure 14. Average volume of sand above threshold elevations (1–6 m above NAVD88) in 2000, 2010, and 2013 for (a) undeveloped segment of southern Padre Island without the road, (b) undeveloped segment with the road, (c) developed segment of southern Padre Island without the retaining wall, and (d) developed segment with the retaining wall.

and migrate in an offshore direction over the winter months (Cheng and Wang, 2018). The bathymetric data comparison recorded migration of the outer sandbar approximately 75 m offshore between October 2012 and February 2013 (Figure 10).

A trend in increasing sediment volume at the lower threshold elevations between the 2000, 2010, and 2013 data sets also reinforces the benefit of the nourishment projects conducted within the City of South Padre Island (Figure 14). The undeveloped segment of southern Padre Island (the largest segment) increased in volume across all of the threshold elevations (Figure 14a). The higher threshold elevations for the undeveloped segment with the road and the developed segment with the retaining wall have kept a fairly constant volume of sand, whereas the lower threshold elevations (1–3 m) are increasing in volume (Figure 14b,d).

The southern Padre Island segment that is developed but without a retaining wall is the only segment where the volume of sand at the higher threshold elevations (>4 m) decreased

Table 5. *Tropical cyclones affecting the southern Texas coast during the study period, where TS = tropical storm; H = hurricane; number following H designates numeric strength according to the Saffir/Simpson scale (Simpson and Riehl, 1981). Data are from the National Oceanic and Atmospheric Administration (NOAA Miami Regional Library, 2017; NOAA National Hurricane Center, 2017) and Roth (2010).*

Year	Category	Name	Begin Date	End Date	Landfall
1945	H4	Unnamed	24 August	29 August	Mustang Island (paralleled coast)
1947	TS	Unnamed	31 July	2 August	Southern Padre Island
1954	H1	Alice	24 June	27 June	S of Rio Grande area
1955	H1	Gladys	5 September	7 September	S of Rio Grande area
1958	TS	Alma	14 June	16 June	S of Rio Grande area
1958	TS	Gerda	14 September	22 September	S of Rio Grande area
1960	TS	Unnamed	22 June	28 June	Padre Island
1961	H5	Carla	3 September	15 September	Matagorda Island
1967	H3	Beulah	5 September	22 September	Brownsville
1970	H3	Celia	31 July	5 August	Corpus Christi
1971	H1	Fern	9 September	13 September	Matagorda Island
1978	TS	Amelia	30 July	31 July	Southern Padre Island
1980	H3	Allen	1 August	11 August	Padre Island
1983	H1	Barry	23 August	29 August	S of Rio Grande area
1988	H4	Gilbert	8 September	19 September	S of Rio Grande area
1993	TS	Arlene	18 June	21 June	Northern Padre Island
1999	H4	Bret	18 August	25 August	Padre Island
2002	TS	Bertha	4 August	9 August	Northern Padre Island
2003	H1	Erika	14 August	17 August	S of Rio Grande area
2005	H5	Emily	11 July	21 July	S of Rio Grande area (H3 at landfall)
2008	H2	Dolly	20 July	25 July	Southern Padre Island
2008	H4	Ike	1 September	15 September	Galveston (H2 at landfall)
2010	H2	Alex	25 June	2 July	S of Rio Grande area
2010	TS	Hermine	5 September	9 September	Rio Grande area
2011	TS	Don	27 July	29 July	Baffin Bay area (TD at landfall)

during the study period (Figure 14c). Construction of buildings in The Shores Subdivision, located within this segment, occurred during the study period. Newer structures in the northernmost portion of this segment were not present in 2000, when the initial LIDAR survey was conducted. Some areas of the dune system that were included in the volume calculations for the 2000 data set were removed due to construction of structures in The Shores Subdivision or other disturbances due to the construction process. Dune mitigation projects and the planting and watering of native dune plants did occur during the construction phase of The Shores Subdivision. Examination of aerial imagery from this segment also reveals an active foredune complex with little vegetative cover prior to construction. Additional sediment at the higher elevations could have been lost to sand being removed from the dunes by wind processes.

Tropical storms and hurricanes have varying effects on Texas Gulf Coast beach and dune systems (*e.g.*, Gibeaut, Gutierrez, and Hepner, 2002; Hayes, 1967; Morton and Paine, 1985; Morton, Paine, and Gibeaut, 1994; Price, 1956). The two critical parameters that increase the erosion potential of a tropical cyclone are surge height and duration. The longer sea level is elevated above normal levels, the greater is the potential for redistribution of sediments from the beach and dune system. Beach and dune recovery after storm passage follows several distinct stages and can extend beyond 2 years after storm landfall (Morton and Paine, 1985; Morton, Paine, and Gibeaut, 1994). Historical lists and records maintained by the National Oceanic and Atmospheric Administration indicate that, on average, four hurricanes and four tropical storms make landfall in Texas per decade (Roth, 2010). Table 5 lists hurricanes (15) and tropical storms (9) that have made landfall on or near southern Padre Island and Brazos Island during the study period (1945–2013). The degree to which the storms impacted the islands depended upon the strength and duration of the storm as well as the storm's landfall location.

Hurricane Bret was a small but powerful hurricane (a category 3 on the Saffir/Simpson scale; Simpson and Riehl, 1981) that made landfall on Padre Island on 23 August 1999 (Lawrence and Kimberlain, 2001). Wind speed at landfall was 185 km/h, storm surge near the center of Bret was estimated at 2.4–3 m, and numerous cuts through the dunes (washover channels) were observed in the northern reaches of the study area (near Mansfield Pass), as well as substantial beach erosion (Lawrence and Kimberlain, 2001). The 2000 LIDAR survey was conducted within a year of Hurricane Bret's landfall. The lower sediment volumes across all threshold elevations, particularly in the undeveloped segments of southern Padre Island (Figure 14a), are likely due to the impacts of Hurricane Bret. Beach and dune recovery, particularly around the storm washover cuts, was still in the initial stages.

Hurricane Ike made landfall in 2008 on the upper Texas coast as a very large category 2 on the Saffir/Simpson scale, causing severe beach erosion to central and upper Texas coast beaches. Ike had an unusually high and long-duration storm surge that elevated water levels along the entire U.S. Gulf of Mexico coast, including a 1–2 m rise in south Texas (Berg, 2009). The storm surge from Ike was higher than the surge associated with category 1 (at landfall) Hurricane Dolly, which made a direct landfall on southern Padre Island in July 2008. The accompanying storm surge during Dolly was about 1 m (Pasch and Kimberlain, 2009). The data collected during the 2010 LIDAR survey allowed for 1.5 years of beach and dune recovery in south Texas after Hurricanes Ike and Dolly.

During the time between the 2010 and 2013 LIDAR surveys, Hurricane Alex (July 2010), Tropical Storm Hermine (September 2010), and Tropical Storm Don (July 2011) made landfalls near the south Texas coast study area. A strong category 2 hurricane, Alex made landfall in NE Mexico on 1 July 2010 (Pasch, 2010). Storm surge was not reported for southern Padre or Brazos Islands but reached a peak of 1–1.5 m on northern Padre Island (Pasch, 2010). Hermine made landfall on the NE coast of Mexico on 7 September 2010 accompanied by winds of 110 km/h and surge heights of 0.5–1.0 m along the southern Texas coast (Avila, 2010). Don weakened to a tropical depression as it made landfall on Padre Island just north of Baffin Bay on 30 July 2011. The maximum recorded surge height was 0.6 m on northern Padre Island (Brennan, 2011).

The tropical cyclones between 2000 and 2013 that made landfall on or near the study area did not have a significant effect on south Texas Gulf Coast shoreline position, as evidenced by the lower retreating shoreline change rate on the decadal scale and the average shoreline advancement during the short-term study period. The beach and dune system quickly recovered to prestorm conditions from any impacts inflicted by these storms, and was aided by sediment contributions from beach nourishment activities that have taken place throughout the study period.

CONCLUSIONS

A topographic and bathymetric LIDAR and aerial imagery survey of southern Padre Island and Brazos Island, Texas, was conducted in February 2013. A high-resolution DEM was constructed from the topographic data, allowing extraction of critical coastal features, including shoreline, potential vegetation line, landward dune boundary, geomorphic units, maximum dune crest elevation and position, and beach and dune volume.

Shoreline change was determined on historical, decadal, and short-term timescales. Historical rates of long-term shoreline change for southern Padre Island and Brazos Island were calculated from shorelines between 1937 and 2013. The shoreline in the study area retreated at 86% of the monitoring sites, with an average rate of 2.2 m/y. Over the period 2000 to 2013, the rates decreased to 1.1 m/y of retreat (76% of sites retreating). Between 2010 and 2013, 64% of monitoring sites advanced an average distance of 4.9 m.

The 2013 DEMs were used to examine beach and dune volumes above threshold elevations ranging from 1 to 6 m. The plots created from the evaluation of the volumes are useful in assessing sand storage, susceptibility to storm-surge flooding, and erosion susceptibility and recovery potential. The total volume of sand in the beach and dune system varied among the different coastal segments (with a lower volume in the developed segments of southern Padre Island and a higher volume in the undeveloped segments). A common trend among the different segments is that volume is incrementally reduced

by approximately half with each 1 m increase in threshold elevation.

The bathymetric data collection portion of this project was the first opportunity to examine the depth capability of the Chiroptera system in the turbid waters along the Gulf of Mexico coast. Definitive seafloor returns were identified in two areas adjacent to the north jetty at Mansfield Channel and the north jetty at Brazos Santiago Pass. In areas where water is more turbid, Chiroptera software misclassified many water-column returns as seafloor returns. Additional analysis of the bathymetric waveforms will be necessary to establish whether true seafloor returns can be extracted from the more turbid 2013 survey areas. This analysis is the subject of active research being conducted jointly by BEG researchers and Leica technicians.

ACKNOWLEDGMENTS

This study was supported by grant no. 13-030-000-6895 from the Texas General Land Office to the Bureau of Economic Geology, The University of Texas at Austin. Tiffany L. Caudle and Thomas A. Tremblay served as the coprincipal investigators. This project was funded under a Coastal Management Program (Cycle 17) grant made available to the State of Texas by the U.S. Department of Commerce, National Oceanic and Atmospheric Administration, pursuant to the Federal Coastal Zone Management Act of 1972, NOAA Award No. NA12NOS4190021. Additional funds were provided by State of Texas Advanced Oil and Gas Resource Recovery (STARR). The following Bureau of Economic Geology staff also contributed to the project: Aaron Averett and Sojan Mathew. Aircraft support for the LIDAR survey was provided by the Texas Department of Transportation. The views expressed herein are those of the authors and do not necessarily reflect the views of the project sponsors. Publication was authorized by the director of the Bureau of Economic Geology, The University of Texas at Austin.

LITERATURE CITED

Arifin, R.R. and Kennedy, A.B., 2011. The evolution of large scale crescentic bars on the northern Gulf of Mexico coast. *Marine Geology*, 285(1–4), 46–58.

Avila, L.A., 2010. *Tropical Storm Hermine (AL102010)*. Miami, Florida: National Oceanic and Atmospheric Administration, National Hurricane Center, *Tropical Cyclone Report*, 17p.

Berg, R., 2009. *Hurricane Ike (AL092008)*. Miami, Florida: National Oceanic and Atmospheric Administration, National Hurricane Center, *Tropical Cyclone Report*, 55p.

Brennan, M.J., 2011. *Tropical Storm Don (AL042011)*. Miami, Florida: National Oceanic and Atmospheric Administration, National Hurricane Center, *Tropical Cyclone Report*, 15p.

Brown, L.F., Jr.; Brewton, J.L.; Evans, T.J.; McGowen, J.H.; White, W.A.; Groat, C.G., and Fisher, W.L., 1980. Environmental geologic atlas of the Texas coastal zone, Brownsville–Harlingen area. Austin, Texas: The University of Texas at Austin, *Bureau of Economic Geology Special Publication*, 140p.

Brutsché, K.E.; Wang, P.; Beck, T.M.; Rosati, J.D., and Legault, K.R., 2014. Morphological evolution of a submerged artificial nearshore berm along a low-wave microtidal coast, Fort Myers Beach, west-central Florida, USA. *Coastal Engineering*, 91, 29–44.

Caudle, T.L., 2017. *Texas High School Coastal Monitoring Program: 2016–2017*. Austin, Texas: University of Texas at Austin, *Bureau of Economic Geology Report Prepared for General Land Office Under Contract 16-067-000-9111 and National Oceanic and Atmospheric Administration Award NA15NOS4190162*, 116p.

Caudle, T.L. and Paine, J.G., 2012. Pre-college student involvement in Texas coastal research. *Gulf Coast Association of Geological Societies Transactions,* 62, 27–38.

Caudle, T.L. and Paine, J.G., 2017. Applications of coastal data collected in the Texas High School Coastal Monitoring Program (THSCMP). *Journal of Coastal Research*, 33(3), 738–746.

Caudle, T.L.; Tremblay, T.A.; Paine, J.G.; Andrews, J.R., and Saylam, K., 2014. *Beach and Dune Analysis Using Chiroptera Imaging System, South Padre and Brazos Island, Texas Gulf Coast*. Austin, Texas: University of Texas at Austin, *Bureau of Economic Geology Report Prepared for General Land Office Under Contract 13-030-000-6895 and National Oceanic and Atmospheric Administration Award NA12NOS4190021*, 68p.

Cheng, J. and Wang, P., 2018. Dynamic equilibrium of sandbar position and height along a low wave energy micro-tidal coast. *Continental Shelf Research*, 165, 120–136.

Chust, G.; Grand, M.; Galparsoro, I.; Uriarte, A., and Borja, Á., 2010. Capabilities of the bathymetric Hawk Eye LiDAR for coastal habitat mapping: A case study within a Basque estuary. *Estuarine, Coastal and Shelf Science*, 89(3), 200–213.

Costa, B.M.; Battista, T.A., and Pittman, S.J., 2009. Comparative evaluation of airborne LiDAR and ship-based multibeam SoNAR bathymetry and intensity for mapping coral reef ecosystems. *Remote Sensing of Environment*, 113(5), 1082–1100.

Gibeaut, J.C. and Caudle, T., 2009. Defining and mapping foredunes, the line of vegetation, and shorelines along the Texas Gulf Coast. Austin, Texas: The University of Texas at Austin, *Bureau of Economic Geology Final Report Prepared for the Texas General Land Office*, 14p.

Gibeaut, J.C.; Gutierrez, R., and Hepner, T., 2002. Threshold conditions for episodic beach erosion along the southeast Texas coast. *Gulf Coast Association of Geological Societies Transactions*, 52, 323–335.

Hayes, M.O., 1967. *Hurricanes as Geological Agents: Case Studies of Hurricanes Carla, 1961 and Cindy, 1963*. Austin, Texas: The University of Texas at Austin, *Bureau of Economic Geology Report of Investigations No. 61*, 54p.

Houser, C. and Barrett, G., 2010. Divergent behavior of the swash zone in response to different foreshore slopes and nearshore states. *Marine Geology*, 271(1–2), 106–118.

Houser, C.; Hapke, C., and Hamilton, S., 2008. Controls on coastal dune morphology, shoreline erosion and barrier island response to extreme storms. *Geomorphology*, 100(3–4), 223–240.

Houser, C. and Mathew, S., 2011. Alongshore variation in foredune height in response to transport potential and sediment supply: South Padre Island, Texas. *Geomorphology*, 125, 62–72.

Kim, H.; Lee, S.B., and Min, K.S., 2017. Shoreline change analysis using airborne LiDAR bathymetry for coastal monitoring. *In:* Lee, J.L.; Griffiths, T.; Lotan, A.; Suh, K.S., and Lee, J. (eds.), *The 2nd International Water Safety Symposium*. *Journal of Coastal Research*, Special Issue No. 79, pp. 269–273.

Kraus, N.C., 2007. Coastal inlets of Texas. *Proceedings Coastal Sediments '07* (New Orleans, Louisiana, Coasts, Oceans, Ports, and Rivers Institute of ASCE), pp. 1475–1488.

Lawrence, M.B. and Kimberlain, T.B., 2001. *Hurricane Bret (AL031999)*. Miami, Florida: National Oceanic and Atmospheric Administration, National Hurricane Center, *Tropical Cyclone Report*, 13p.

McGowen, J.H.; Garner, L.E., and Wilkinson, B.H., 1977. *The Gulf Shoreline of Texas: Processes, Characteristics and Factors in Use*. Austin, Texas: The University of Texas at Austin, *Bureau of Economic Geology Geological Circular 77-3,* 27p.

Moore, L.J.; Ruggiero, P., and List, J.H., 2006. Comparing mean high water and high water line shorelines: Should proxy-datum offsets be incorporated into shoreline change analysis? *Journal of Coastal Research*, 22(4), 894–905.

Morton, R.A., 1977. Historical shoreline changes and their causes, Texas Gulf Coast. *Gulf Coast Association of Geological Societies Transactions*, 27, 352–364.

Morton, R.A.; Miller, T.L., and Moore, L.J., 2004. *National Assessment of Shoreline Change, Part 1: Historical Shoreline Changes and Associated Coastal Land Loss Along the U.S. Gulf of Mexico*. St. Petersburg, Florida: U.S. Geological Survey, *Open-File Report 2004-1043*, 42p.

Morton, R.A.; Miller, T.L., and Moore, L.J., 2005. Historical shoreline changes along the US Gulf of Mexico: A summary of recent shoreline comparisons and analyses. *Journal of Coastal Research*, 21(4), 704–709.

Morton, R.A. and Paine, J.G., 1985. *Beach and Vegetation-line Changes at Galveston Island, Texas: Erosion, Deposition, and Recovery from Hurricane Alicia*. Austin, Texas: The University of Texas at Austin, *Bureau of Economic Geology Geological Circular 85-5*, 39p.

Morton, R.A. and Paine, J.G., 1990. Coastal land loss in Texas: An overview. *Gulf Coast Association of Geological Societies Transactions*, 40, 625–634.

Morton, R.A.; Paine, J.G., and Gibeaut, J.C., 1994. Stages and durations of post-storm beach recovery, southeastern Texas coast, U.S.A. *Journal of Coastal Research*, 10(4), 884–908.

Morton, R.A. and Pieper, M.J., 1975. *Shoreline Changes on Brazos Island and South Padre Island (Mansfield Channel to Mouth of the Rio Grande), an Analysis of Historical Changes of the Texas Gulf Shoreline*. Austin, Texas: The University of Texas at Austin, *Bureau of Economic Geology Geological Circular 75-2*, 39p.

National Geodetic Survey, 2012. https://www.ngs.noaa.gov/GEOID/GEOID12A.

NOAA Miami Regional Library, 2017. *Monthy Weather Review – Annual Summaries of North Atlantic Storms, 1872-2011*. http://www.aoml.noaa.gov/general/lib/lib1/nhclib/mwreviews.html.

NOAA National Hurricane Center, 2017. *Tropical Cyclone Reports*, https://www.nhc.noaa.gov/data/.

Paine, J.G.; Andrews, J.R.; Saylam, K., and Tremblay, T.A., 2015. Airborne LIDAR-based wetland and permafrost-feature mapping on an Arctic coastal plain, North Slope, Alaska. *In*: Tiner, R.W.; Lang, M.W., and Klemas, V.V. (eds.), *Remote Sensing of Wetlands: Applications and Advances*. Boca Raton, Florida: CRC Press, pp. 413–434.

Paine, J.G.; Andrews, J.R.; Saylam, K.; Tremblay, T.A.; Young, M.H.; Abolt, C.; Bradford, B.; Caudle, T.; Meyer, T., and Neuenschwander A., 2013. *Determining Wetlands Distribution, Lake Depths, and Topography using Airborne LIDAR and Imagery on the North Slope, Deadhorse Area, Alaska*. Austin, Texas: The University of Texas at Austin, *Bureau of Economic Geology Final Technical Report Prepared for Great Bear Petroleum Operating LLC Under Sponsored Research Agreement UTA12-0000752*, 88p.

Paine, J.G.; Caudle, T.L., and Andrews, J.R., 2013. *Shoreline, Beach, and Dune Morphodynamics, Texas Gulf Coast*. Austin, Texas: The University of Texas at Austin, *Bureau of Economic Geology Final Report Prepared for General Land Office Under Contract 09-242-000-3789*, 64p.

Paine, J.G.; Caudle, T.L., and Andrews, J.R., 2014. *Shoreline Movement along the Texas Gulf Coast, 1930's to 2012*. Austin, Texas: The University of Texas at Austin, *Bureau of Economic Geology Final Report Prepared for General Land Office Under Contract 09-074-000*, 52p.

Paine, J.G.; Caudle, T.L., and Andrews, J.R., 2017. Shoreline and sand storage dynamics from annual airborne LIDAR surveys, Texas Gulf Coast. *Journal of Coastal Research*, 33(3), 487–506.

Paine, J.G.; Mathew, S., and Caudle, T., 2011. *Texas Gulf Shoreline Change Rates Through 2007*. Austin, Texas: University of Texas at Austin, *Bureau of Economic Geology Report Prepared for General Land Office Under Contract 10-041-000-3737 and National Oceanic and Atmospheric Administration Award NA09NOS4190165*, 38p.

Paine, J.G.; Mathew, S., and Caudle, T., 2012. Historical shoreline change through 2007, Texas Gulf Coast: Rates, contributing causes, and Holocene context: *Gulf Coast Association of Geological Societies Journal*, 1, 13–26.

Paine, J.G. and Morton, R.A., 1989. *Shoreline and Vegetation-line Movement, Texas Gulf Coast, 1974 to 1982*. Austin, Texas: The University of Texas at Austin, *Bureau of Economic Geology Geological Circular 89-1*, 50p.

Pasch, R.J., 2010. *Hurricane Alex (AL012010)*. Miami, Florida: National Oceanic and Atmospheric Administration, National Hurricane Center, *Tropical Cyclone Report*, 19p.

Pasch, R.J. and Kimberlain, T.B., 2009. *Hurricane Dolly (AL042008)*. Miami, Florida: National Oceanic and Atmospheric Administration, National Hurricane Center, *Tropical Cyclone Report*, 19p.

Pastol, Y., 2011. Use of airborne LIDAR bathymetry for coastal hydrographic surveying: The French experience. *In:* Pe'eri, S. and Long, B. (eds.), *Applied LIDAR Techniques*. *Journal of Coastal Research,* Special Issue No. 62, pp. 6–18.

Perry, M.C., 2013. *Monitoring Survey of South Padre Island 2013 Annual Beach Report*. Corpus Christi, Texas: HDR Engineering, Inc., *Report Prepared for Texas General Land Office*, 10p.

Perry, M.C., 2014. *Annual Monitoring Survey of South Padre Island Beach*. Corpus Christi, Texas: HDR Engineering, Inc., *Report Prepared for City of South Padre Island*, 14p.

Preisendorfer, R.W., 1986. Secchi disk science: Visual optics of natural waters. *Limnology and Oceanography*, 31(5), 909–926.

Price, W.A., 1956. *Hurricanes Affecting the Coast of Texas from Galveston to the Rio Grande*. Washington, D.C.: U.S. Army Corps of Engineers, *Beach Erosion Board Technical Memorandum 78*, 35p.

Revell, D.L.; Komar, P.D., and Sallenger, A.H., Jr., 2002. An application of LIDAR to analyses of El Niño erosion in the Netarts littoral cell, Oregon. *Journal of Coastal Research*, 18(4), 792–801.

Roberts, T.M. and Wang, P., 2012. Four-year performance and associated controlling factors of several beach nourishment projects along three adjacent barrier islands, west-central Florida, USA. *Coastal Engineering*, 70, 21–39.

Roth, D., 2010. *Texas Hurricane History*. Camp Springs, Maryland: National Weather Service, 83p. http://origin.wpc.ncep.noaa.gov/research/txhur.pdf.

Ruggiero, P.; Walstra, D.J.R.; Gelfenbaum, G., and van Ormondt, M., 2009. Seasonal-scale nearshore morphological evolution: Field observations and numerical modeling. *Coastal Engineering*, 56(12), 1153–1172.

Sallenger, A.H., Jr.; Krabill, W.B.; Swift, R.N.; Brock, J.; List, J.; Hansen, M.; Holman, R.A.; Manizade, S.; Sontag, J.; Meredith, A.; Morgan, K.; Yunkel, J.K.; Frederick, E.B., and Stockdon, H., 2003. Evaluation of airborne topographic LIDAR for quantifying beach changes. *Journal of Coastal Research*, 19(1), 125–133.

Saylam, K.; Hupp, J.R.; Averett, A.R.; Gutelius, W.F., and Gelhar, B.W., 2018. Airborne LIDAR bathymetry: Assessing quality assurance and quality control methods with Leica Chiroptera examples. *International Journal of Remote Sensing*, 39(8), 2518–2542.

Shalowitz, A.L., 1964. *Shore and Beach Boundaries*. Washington, D.C.: U.S. Department of Commerce, *Publication 10-1*, 749p.

Simpson, R.H. and Riehl, H., 1981. *The Hurricane and its Impact*. Baton Rouge, Louisiana: Louisiana State University Press, 398p.

Stockdon, H.F.; Doran, K.S., and Sallenger, A.H., Jr., 2009. Extraction of LIDAR-based dune-crest elevations for use in examining the vulnerability of beaches to inundation during hurricanes. *In:* Brock, J.C. and Purkis, S.J. (eds.), *Coastal Applications of Airborne Lidar Remote Sensing*. *Journal of Coastal Research*, Special Issue, No. 53, pp. 59–65.

Stockdon, H.F.; Sallenger, A.H., Jr.; List, J.H., and Holman, R.A., 2002. Estimation of shoreline position and change using airborne topographic LIDAR data. *Journal of Coastal Research*, 18(3), 502–513.

Texas Natural Resource Code, 1991. *Title 2, Subtitle E, § 61.001*. https://statutes.capitol.texas.gov/Docs/NR/htm/NR.61.htm

Thatcher, C.A.; Brock, J.C.; Danielson, J.J.; Poppenga, S.K.; Gesch, D.B.; Palaseanu-Lovejoy, M.E.; Barras, J.A.; Evans, G.A., and Gibbs, A.E., 2016. Creating a Coastal National Elevation Database (CoNED) for science and conservation applications. *In:* Brock, J.C.; Gesch, D.B.; Parrish, C.E.; Rogers, J.N., and Wright, C.W. (eds.), *Advances in Topobathymetric Mapping, Models, and Applications*. *Journal of Coastal Research,* Special Issue No. 76, pp. 64–74.

Thieler, E.R.; Himmelstoss, E.A.; Zichichi, J.L., and Ergul, A., 2009. *Digital Shoreline Analysis System (DSAS) Version 4.0—An ArcGIS Extension for Calculating Shoreline Change*. Woods Hole, Massachusetts: U.S. Geological Survey, *Open-File Report 2008-1278*.

Tyler, J.E., 1968. The Secchi disc. *Limnology and Oceanography*, 13(1), 1–6.

Weber, K.M.; List, J.H., and Morgan, K.L.M., 2005. *An Operational Mean High Water Datum for Determination of Shoreline Position from Topographic LIDAR Data*. U.S. Geological Survey, *Open-File Report 2005-1027* (Woods Hole, Massachusettes). https://pubs.usgs.gov/of/2005/1027/index.html.

Webster, T.; McGuigan, K.; Crowell, N.; Collins, K., and MacDonald, C., 2016. Optimization of data collection and refinement of post-processing techniques for Maritime Canada's first shallow water topographic-bathymetric LIDAR survey. *In:* Brock, J.C.; Gesch, D.B.; Parrish, C.E.; Rogers, J.N., and Wright, C.W. (eds.), *Advances in Topobathymetric Mapping, Models, and Applications*. *Journal of Coastal Research,* Special Issue No. 76, pp. 31–43.

Williams, D.D. and Kraus, N.C., 2011. Seasonal change in nearshore and channel morphology at Packery Channel, a new inlet serving Corpus Christi, Texas. *In:* Roberts, T.M.; Rosati, J.D., and Wang, P. (eds.), *Proceedings, Symposium to Honor Dr. Nicholas C. Kraus*. *Journal of Coastal Research,* Special Issue No. 59, pp. 86–97.

Woolard, J.W. and Colby, J.D., 2002. Spatial characterization, resolution, and volumetric change of coastal dunes using airborne LIDAR: Cape Hatteras, North Carolina. *Geomorphology*, 48, 269–287.

Wozencraft, J. and Lillycrop, W.J., 2006. JALBTCX coastal mapping for the USACE. *International Hydrographic Review,* 7, 28–37.

Wozencraft, J. and Millar, D., 2005. Airborne LIDAR and integrated technologies for coastal mapping and nautical charting. *Marine Technology Society Journal*, 39(3), 27–35.

Wright, C.W.; Kranenburg, C.; Battista, T.A., and Parrish, C., 2016. Depth calibration and validation of the Experimental Advanced Airborne Research LIDAR, EAARL-B. *In:* Brock, J.C.; Gesch, D.B.; Parrish, C.E.; Rogers, J.N., and Wright, C.W. (eds.), *Advances in Topobathymetric Mapping, Models, and Applications*. *Journal of Coastal Research,* Special Issue No. 76, pp. 4–17.

Xhardé, R.; Long, B.F., and Forbes, D.L., 2011. Short-term beach and shoreface evolution on a cuspate foreland observed with airborne topographic and bathymetric LIDAR. *In:* Pe'eri, S. and Long, B. (eds.), *Applied LIDAR Techniques*. *Journal of Coastal Research,* Special Issue No. 62, pp. 50–61.